Journal of Molecular Structure 1102 (2015) 295–301

Contents lists available at ScienceDirect

Journal of Molecular Structure

journal homepage: http://www.elsevier.com/locate/molstruc

# Synthesis, X-ray crystal structures and catecholase activity investigation of new chalcone ligands

Salima Thabti [a, b], Amel Djedouani [c, d], Samra Rahmouni [b], Rachid Touzani [e, f], Abderrahmen Bendaas [b], Hénia Mousser [c, d, *], Abdelhamid Mousser [c, d]

[a] Faculté des Sciences et Technologie, Université Mohamed el Bachir El Ibrahimi, El Anasser, 34000, Bordj Bou Arréridj, Algeria
[b] Laboratoire de Matériaux Moléculaires et Complexes, Université Ferhat ABBAS, Sétif, 19000, Algeria
[c] Laboratoire de Physicochimie Analytique et Cristallochimie des Matériaux Organométalliques et Biomoléculaires, Université Constantine 1, 25000, Constantine, Algeria
[d] Ecole Normale Supérieure de Constantine, Ville Universitaire Ali Mendjeli, 25000, Constantine, Algeria
[e] Laboratoire de Chimie Appliquée et Environnement, LCAE-URAC18, COSTE, Faculté des Sciences, Université Mohamed Premier, BP524, 60000, Oujda, Morocco
[f] Faculté Pluridisciplinaire Nador BP 300, Selouane, 62702, Nador, Morocco

ARTICLE INFO

*Article history:*
Received 5 June 2015
Received in revised form
28 August 2015
Accepted 31 August 2015
Available online 4 September 2015

*Keywords:*
Synthesis
Chalcone
X-ray crystal structure
Oxidation
Transition metal
$O_2$ activation

ABSTRACT

The reaction of dehydroacetic acid DHA carboxaldehyde and RCHO derivatives (R = quinoleine−8−; indole−3−; pyrrol−2− and 4−(dimethylamino)phenyl − afforded four new chalcone ligands (4−hydroxy −6−methyl−3−[(2*E*)−3−quinolin−8−ylprop−2−enoyl]−2H−pyran−2−one) **L1**, (4−hydroxy−3−[(2*E*) −3−(1H−indol−3−yl)prop−2−enoyl]−6−methyl−2H−pyran−2−one) **L2**, (4−hydroxy−6−methyl−3 −[(2*E*)−3−(1H−pyrrol−2−yl)prop−2−enoyl]−2H−pyran-2-one) **L3**, and (3−{(2E)−3−[4−(dimethylamino)phenyl]prop−2−enoyl}−4−hydroxy−6−methyl−2H−pyran−2−one) **L4**. **L3** and **L4** were characterized by X-ray crystallography. Molecules crystallize with four and two molecules in the asymmetric unit, respectively and adopt an *E* conformation about the C=C bond. Both structures are stabilized by an extended network O−H … O. Furthermore, N−H … O and C−H … O hydrogen bonds are observed in **L3** and **L4** structures, respectively. The in situ generated copper (II) complexes of the four compounds **L1**, **L2**, **L3** and **L4** were examined for their catalytic activities and were found to catalyze the oxidation reaction of catechol to *o*-quinone under atmospheric dioxygen. The rates of this oxidation depend on three parameters: ligand, ion salts and solvent nature and the combination **L2**[Cu $(CH_3COO)_2$] leads to the faster catalytic process.



## 1. Introduction

The oxidation of organic substrates with molecular oxygen under mild conditions is of great interest for industrial and synthetic processes both from an economical and environmental point of view [1,2]. The synthesis and investigation of functional model complexes for metalloenzymes with oxidase or oxygenase activity is therefore of great promise for the development of new and efficient catalysts for oxidation reactions [3]. Copper has been known as a bio-essential element for a long time [4], but its biological relevance was fully recognized only in the previous years due to the development of its bioinorganic chemistry and successful interaction between the chemistry complex models and metal-protein biochemistry [4–12]. It is now well known that proteins containing copper (metal-protein) play a very important role in transport, activation, and metabolism of dioxygen in living organisms [13]. Several catechol derivative substrates were used in the literature to understand the mechanisms of oxidase enzyme research [14]. Catechol oxidase (CO) are plant enzymes [15] which catalyze the oxidation of a broad range of o-diphenols to o-quinones in presence of dioxygen [14–16] through the four-electron reduction of molecular oxygen to water [17–20]. It was observed that the catalytic activities of the complexes are not only dependent on the organic ligand but also on the type of inorganic anion coordinated to the copper center [21]. In this paper, we report the

* Corresponding author. Ecole Normale Supérieure de Constantine, Laboratoire de Physicochimie Analytique et Cristallochimie des Matériaux Organométalliques et Biomoléculaires, Université Constantine 1, 25000, Constantine, Algeria.
*E-mail address:* bouzidi_henia@yahoo.fr (H. Mousser).

http://dx.doi.org/10.1016/j.molstruc.2015.08.071
0022-2860/

synthesis of four new chalcone derivatives of dehydroacetic acid (Scheme 1) and describe their in situ generated copper (II) complexes catecholase activity.

## 2. Experimental

### 2.1. Materials and physical measurements

All reagents and solvents were analytical grade and used without further purification. Elemental analyses were carried out by the service central of analyses (C.N.R.S. Vernaison, France) by Std. meth.0804-ox, with K Factors calibration.

The melting points were determined with a Kofler bank and are not corrected. The FT-IR spectra (4000–400 $cm^{-1}$) are recorded from KBr disks using FT-IR-4000 (Shimadzu) spectrophotometer. $^{1}$HNMR (300 MHz) and $^{13}$C NMR (400 MHz) spectra were recorded using $CDCl_3$ and tetramethylsilane (TMS) was used as an internal reference. The electronic spectra of the ligand and its metal complexes were measured on a UV PROB SHIMADZU 1700 spectrophotometer in the range of 200–900 nm.

### 2.2. X-ray crystallographic study

X-ray single-crystal diffraction data were collected at 293 K on a Diffractomètre Bruker-Nonius and goniomètre Kappa CCD, equipped with a graphite monochromator using Mo/Kα radiation (λ = 0.71073 Å) (Spectropole-RX, Campus Saint-Jérôme, Service D11, Aix-Marseille Université). Structures were solved by direct methods and refined on F2 by full-matrix least-squares method, using SHELX97 package [22]. All non-H atoms were refined anisotropically by the full matrix least squares method on F2 using SHELXL [23] and the H atoms were included at the calculated positions and constrained to ride on their parent atoms.

### 2.3. Catecholase activity measurements

Kinetic measurements were made spectrophotometrically on UV–Vis spectrophotometer, following the appearance of *o*-quinone over time at 25 °C (390 nm absorbance maximum, ε = 1600 L $mol^{-1}$ $cm^{-1}$ in methanol [24]). The complexes were prepared in situ by successively mixing 0.15 mL of a solution ($2 \times 10^{-3}$ M) of $CuX_2$, $nH_2O$ (X = $Cl^-$, $Br^-$, $NO_3^-$, $CH_3COO^-$ or $SO_4^{2-}$), with 0.15 mL of a solution ($2 \times 10^{-3}$ M) of ligand, then adding 2 mL of a solution of catechol at a concentration of $10^{-1}$ M.

### 2.4. Synthesis and characterization

All compounds were prepared as described elsewhere [25–28].

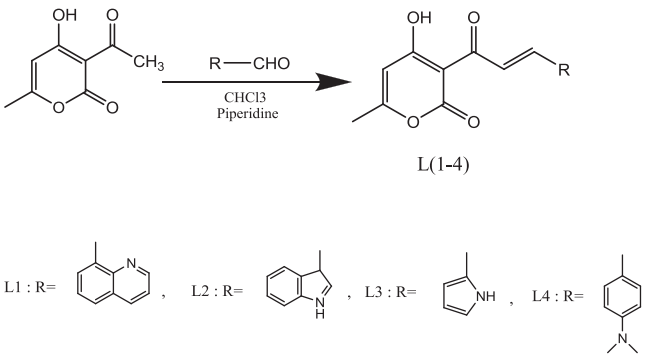


**Scheme 1.** .

A mixture of dehydroacetic acid (1.68 g; 0.01 mol) and R-carboxaldehyde (0.01 mol) were refluxed in 25 ml of chloroform containing a few drops of piperidine. 5–7 ml of the chloroform-water azeotrope mixture was removed by a simple distillation. The product were obtained by slow evaporation of the remaining chloroform and washed with ethyl acetate (2 × 5 ml). **L3** and **L4** were recrystalized from dichloromethane and a mixture of Ethanol and a few drops of DMSO, respectively. Crystals were dried under vaccum.

#### 2.4.1. 4-hydroxy-6-methyl-3-[(2E)-3-quinolin-8-ylprop-2-enoyl]-2H-pyran-2-one (*L1*)

$^{1}$H NMR($CDCl_3$): *δ ppm*: 2.18 (s, 3H, $CH_3$); 5.99 (s, 1H, C=CH–C=$C_{Pyr}$); 7.48–7.93 (m, 3H, CH–CH=$CH_{Aryl}$); 8.29 (dd, 2H, CH=$CH_{Eth}$); 8.59–9.38 (m, 3H, CH–CH=$CH_{Quin}$); 11.48 (s, 1H, OH). $^{13}$C RMN($CDCl_3$): *δ ppm*: 20.67 ($CH_3$); 99.61 (N=CH); 102.61 (C=CH); 121.68 (C–$C_{Quin}$ = C); 124.55 (N–C=$C_{Quin}$); 126.40 (CO–C = ); 128.47 ($CH_{Quin}$); 128.61 ($CH_{Quin}$); 130.96 ($C_{Quin}$); 133.28 ($C_{Quin}$); 136.29 ($CH_{Quin}$); 142.62 ($C_{Quin}$); 146.56 ($CH_{Quin}$); 150.44 (CH=$C_{Quin}$); 161.41 (CO); 168.49 (C–$CH_3$); 183.40 (C–OH); 192.83(CO). IR (KBr, ν $cm^{-1}$): 3400 (OH, Pyr); 1650 (C=N, Quin); 1520 (C=C, Aryl); 1700 (C=O); 1000 (C–O, Pyr). $[M]^+$ Calc. $C_{18}H_{13}NO_4$: *m/z* = 307.0845; peaks selected for the internal calibration are observed: *m/z* = 300.2017 and *m/z* = 327.2013, respectively.

#### 2.4.2. 4-hydroxy-3-[(2E)-3-(1H-indol-3-yl) prop-2-enoyl]-6-methyl-2H-pyran-2-one: (*L2*)

$^{1}$H NMR ($CDCl_3$): *δ ppm*: 2,23 (s, 3H, $CH_3$); 6.18 (s, $1H_{Pyr}$); 7.28–7.96 (m, 4H, CH=CH–CH=$CH_{Aryl}$); 8.16 (d, 1H, $CH_{Ind}$); 8.22 (d, 2H, CH=$CH_{Ethyl}$); 8.33 (d, 1H, -$NH_{Ind}$); 12.19 (S, 1H, OH). *$^{13}$C NMR (DMSO)* *δ* ppm: 19.93 ($CH_3$); 97.97 (C=$C_{Pyr}$); 102.62 (C=$CH_{Pyr}$–C); 113 (C–$CH_{Ind}$); 113.78 (CH $_{Ind}$ = C–N); 114.65 (CH=C)$_{Ind}$; 120.08 (CH=C)$_{Ind}$; 122.04 (CH=C)$_{Ind}$; 123.42 (CH–C–CH)$_{Ind}$; 124.66 (HC–N); 136.64 (CH=CH) $_{Ethy}$; 137.98 (C–NH); 142.43 (CH=CH)$_{Ethy}$; 160.91, 168.5 (C–$CH_3$); 183.49 (C–OH); 190.41 (CO). IR (KBr, ν $cm^{-1}$): 3400 (OH, Pyr); 1650 (C=N, Ind); 1520 (C=C, Aryl); 1700 (C=O); 1000 (C–O, Pyr); 3100 (C–H). [M] $^+$ Calc. $C_{18}H_{13}NO_4$: *m/z* = 307.0845; peaks selected for the internal calibration are observed: *m/z* = 300.2017 and *m/z* = 327.2013, respectively.

#### 2.4.3. 4-hydroxy-6-methyl-3-[(2E)-3-(1H-pyrrol-2-yl) prop-2-enoyl]-2H-pyran-2-one (*L3*)

$^{1}$H NMR ($CDCl_3$): *δ ppm*: 2,13 (s, 3H, $CH_3$); 3.58 (d, 1H, N–H); 5.72 (s, 1H, N–$CH_{Pyr}$); 6.18 (s, $1H_{Py}$); 6.54 (s, 2H, =$CH_{Pyr}$); 6.91 (s, CH = ); 7.29(s, =CH); 11.8 (s, OH). $^{13}$C NMR (DMSO): *δ ppm*: 21 ($CH_3$); 101 (C=$C_{Pyr}$); 102 (C=$CH_{Pyr}$–C); 108.3(C=$C_{Pyr}$); 11.8(CH=CH); 118.3 (CH $_{Pyr}$ = C–N); 129 (CH=CH)$_{Ethy}$; 129.5 (HC–N); 143.5 (CH=CH)$_{Ethy}$; 162.6 (C–$CH_3$); 163 (CO); 183.8 (CO); 191.1 (C–OH). IR (KBr, ν $cm^{-1}$): 3400 (OH, Pyr); 3100 (N–H); 2850 (C–$H_{Aryl}$); 1700 (C=O, Pyr); 1650 (C=N); 1700 (C=O); 1000 (C–O, Pyr). [M] $^+$ Calc. $C_{13}H_{11}O_4N$: *m/z* = 245.1900; peaks selected for the internal calibration are observed: *m/z* = 245.2017 and *m/z* = 245.2013, respectively.

#### 2.4.4. 3-{(2E)-3-[4-(dimethylamino)phenyl]prop-2-enoyl}-4-hydroxy-6-methyl-2H-pyran-2-one (*L4*)

$^{1}$H NMR ($CDCl_3$): *δ ppm*: 2.18 (s, 3H, $CH_3$); 3 (s, 6H, $CH_3$–N–$CH_3$); 5.83 (s, 1H, $CH_{Pyr}$); 6.60 (s, 1H, $CH_{Aryl}$); 6.63 (s, 1H, $CH_{Aryl}$); 7.53 (s, 1H, $CH_{Aryl}$); 7.55 (s, 1H, $CH_{Aryl}$); 7.93 (d, 1H, CH=$CH_{Ethy}$, J = 15.5 Hz); 8.05 (d, 1H, CH=$CH_{Ethy}$, J = 15.5 Hz). $^{13}$C NMR (DMSO): *δ ppm*: 20.53 ($CH_3$); 40.12 ($H_3C$–N); 98.98 (C=C); 103.19 (C–$H_{Pyr}$); 111.77 (C–$H_{Aryl}$); 116.40 (CH=CH–$C_{Aryl}$); 122.67 (CH=CH)$_{Ethy}$; 131.81 ($CH_{Aryl}$); 148.32 (CH=CH)$_{Ethy}$; 152.70 ($CH_{Aryl}$–N); 161.61 (CO); 167.38 (C–O) $_{Pyr}$; 183.93 (C–OH); 191.93 (CO). IR (KBr, ν $cm^{-1}$):

3400 (OH, Pyr); 1700 (C=O, Pyr); 1650 (C=N); 1700 (C=O); 1000 (C–O, Pyr); [M] $^{+}$ Calc. $C_{17}H_{17}NO_4$: $m/z$ = 300.1229; peaks selected for the internal calibration are observed $m/z$ = 309.2272 and $m/z$ = 327.2013, respectively.

## 3. Results and discussion

### 3.1. Reaction of DHA with RCHO

Dehydroacetic acid reacted with four carboxaldehydes RCHO (Scheme 1) and afforded four colored chalcones: **L1** (80%); **L2** (70%); **L3** (75%) and **L4** (80%). Obtained compound were fully characterized by mass spectrometry and by spectroscopic methods. In the other hand, **L3** and **L4** were characterized by X-ray crystallography. The formation of **L(1–4)** is the result of a Claisen–Schmidt condensation of DHA and RCHO derivatives. Elemental analyses are in good agreement with the experimental result. The $^{1}$HNMR spectrums in CDCl3, with TMS as an internal standard, showed a singlet between 2.13 and 2.23 ppm for methyl group hydrogens attached to the DHA ring, a singlet between 5.83 and 6.18 ppm for hydrogen of the DHA ring, a singlet between 11.4 and 11.8 ppm for the phenolic hydrogen and a doublet between 7.2 and 7.9 ppm for the two olefinic protons. The IR spectra of ligands show bands at 3400–3100, 1700, 1520–1550 and 1650–1675 cm$^{-1}$ assignable to ν(OH) (phenolic hydrogen bonded), ν(C=O) (lactone carbonyl), ν(C–O) (phenolic) and ν(C=O) (acetyl carbonyl) stretching mode, respectively. Additional analytical data of **L1**, **L2**, **L3** and **L4** are summarized in Table 1.

### 3.2. Crystallographic studies

#### 3.2.1. Crystal structure description of L3

Orange crystals of **L3** were grown in ethanol. Crystals are monoclinic with space group $P2_1/n$. Structure of **L3** is illustrated in Fig. 1. The main crystal parameters are reported in Table 2. The molecule of **L3** adopts *E* configuration with respect to the $C_7$–$C_8$ double bond. The molecule is quite planar and the angle between the two ring planes is 4.71°. To the $C_7$–$C_8$ double bond, the atom pairs $C_6/C_9$, $H_7/H_8$ are all *trans*, shown by the value of 2.38 (14)° for $O_4$–$C_6$–$C_7$–$C_8$ torsion angle. The double-bond character of the bond between $C_7$ and $C_8$ is deduced from the short bond distance 1.344 (3) Å (Table 3). Molecules of **L3** exhibit one intramolécular hydrogen bonds $O_3$–$H_3$ … $O_4$ and two intermolecular Hbonds $N_1$–$H_1$ … O2 and $C_{10}$–$H_{10}$ … $O_4$ (Fig. 2, Table 4). In the crystal, molecules are aligned head to foot along *b* axis, forming layers that extend in zigzag parallel to the plane (a, b), (Fig. 2).

#### 3.2.2. Crystal structure description of L4

The main crystal parameters are reported in Table 2. The molecule of **L4** with numbering scheme is given in Fig. 3. The compound exists in an *E* configuration with respect to the $C_7$–$C_8$ double bonds.

The molecule is not planar and the angle between the two rings derived from DHA and phenyl is 11.83°. To the C07–C08 bond, the atom pairs C06/C09, H07/H08 are all *trans*, shown by the value of −3.51 (14)° for O04–C06–C07–C08 torsion angle.

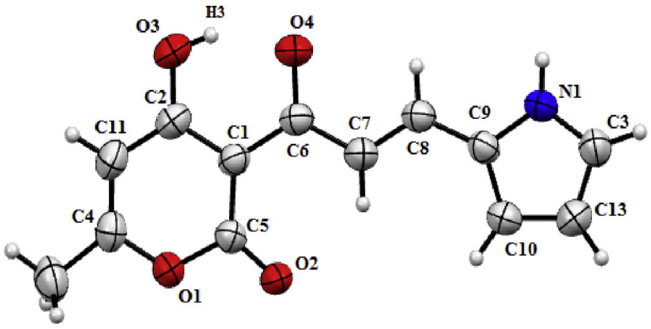


**Fig. 1.** Crystal structure and atoms numbering for **L3**.

The double-bond character of the bond between C07 and C08 is deduced from the short bond distance 1.348 (3) Å (Table 3). Structure of **L4** is stabilized by five hydrogen bonds an intramolecular interaction: O02–H02 … O01 and four intermolecular H bonds: C04–H04 … O02, C015–H015 … O01, C016–H018 … O03 and C017–H017 … O04 (Fig. 4, Table 4). The stacking of molecules within the crystal lattice generates double zigzag planes parallel to the plane (*b*, *c*) (Fig. 4).

All bond lengths and angles in **L3** and **L4** have normal values [29]. The hydroxyl hydrogen, participates in a strong intramolecular hydrogen bond with the carbonyl atom (Table 4) and generates an S (6) ring motif [30]. Similar intramolecular hydrogen bonds were reported in the above-mentioned zwitterionic phenolates [31]. This six-membered pseudocycle is almost planar and the cohesion of the two crystals is ensured by the presence of intermolecular hydrogen bonds.

### 3.3. Catecholase studies

The progress of the catechol oxidation reaction is conveniently followed by monitoring the strong absorbance peak of *o*-quinone in the UV/Vis spectrophotometer (Scheme 2). The metal complex solution and catechol reductant were added together in the spectrophotometric cell at 25 °C [32–35] (1 equivalent of ligand for 1 equivalent of metallic salt). Formation of *o*-quinone was monitored by the increase in absorbance at 390 nm as a function of time. In all cases, catecholase activity was noted. Table 5 gives absorbances of Cu(II) complexes generated in situ after 60 min by mixing metallic salts $Cu(CH_3COO)_2$, $Cu(Br)_2$, $Cu(Cl)_2$, $Cu(NO_3)_2$ and $CuSO_4$ and ligands L1–L4 (1/1) and catechol. The oxidation rates are shown in Table 6.

It appears clearly that catalytic activity varies from one complex to another. All copper complexes, catalyze the oxidation reaction of catechol to *o*-quinone, but with oxidation rate values ranging from 0.035 μmol L$^{-1}$ min$^{-1}$, for complex formed from **L1** and metallic salt $CuCl_2$ (weak catalyst), to 31.78 μmol L$^{-1}$ min$^{-1}$, for complex formed from ligand **L2** and metallic salt $Cu(CH_3COO)_2$ (best catalyst)

**Table 1**
Analytical data for the ligands **L1**, **L2**, **L3** and **L4**.

| Compound | FW (g/mol) | Color | MP (°C) | Rdt | Found (calc)% | | | |
|---|---|---|---|---|---|---|---|---|
| | | | | | C | H | O | N |
| **L1**($C_{18}H_{13}O_4N$) | 307.08 | Olive powder | 215 | 80 | 70.11 (70.33) | 4.41 (4.23) | 20.19 (20.84) | 4.90 (4.55) |
| **L2**($C_{17}H_{13}O_4N$) | 295.08 | Orange Powder | 224.7 | 70 | 65.04 (69.15) | 4.05 (4.74) | 20.14 (21.69) | 4.42 (4.47) |
| **L3**($C_{13}H_{11}O_4N$) | 245 | Orange crystal | 225 | 75 | 63.21 (63.67) | 4.85 (4.48) | 26.01 (26.12) | 5.95 (5.71) |
| **L4**($C_{17}H_{17}O_4N$) | 299 | Red crystal | 222 | 80 | 68.65 (68.22) | 5.76 (5.98) | 20.59 (21.40) | 4.72 (4.68) |

**Table 2**
Crystallographic data and structure refinement details for **L3** and **L4**.

| Name | L3 | L4 |
|---|---|---|
| Formula | $C_{13}H_{11}NO_4$ | $C_{17}H_{17}NO_4$ |
| Formula weight | 245.23 | 299.31 |
| Crystal color | Orange | Red |
| Space group | $P2_1/n$ | $P2_1$ |
| $F$ (000) | 512 | 316 |
| Crystal system | Monoclinic | Monoclinic |
| **Unit cell dimensions** | | |
| a (Å) | 8.96322 (15) | 10.5409 (12) |
| b (Å) | 12.25193 (16) | 4.02669 (7) |
| c (Å) | 10.37846 (2) | 17.2101 (2) |
| β (°) | 93.0584 (15) | 97.0943 (11) |
| V (Å$^3$) | 1138.11 (3) | 725.177 (18) |
| Z | 4 | 2 |
| Temperature(K) | 293 (2) | 293 (2) |
| θ Range for data collection (°) | 5.6–73.6° | 4.2–73.6 |
| Crystal size (mm) | 0.2 × 0.2 × 0.08 | 0.2 × 0.16 × 0.14 |
| Wavelength ((Cu $K\alpha$) (Å) | 1.54184 | 1.54184 |
| $D_{calc}$ (g cm$^{-3}$) | 1.431 | 1.371 |
| μ(mm$^{-1}$) | 0.901 | 0.808 |
| *hkl* range | $-10 \le h \le 11$<br>$-15 \le h \le 15$<br>$-12 \le h \le 12$ | $-13 \le h \le 13$<br>$-4 \le k \le 413$<br>$-21 \le l \le 21$ |
| Ref Nmb of reflections measured | 17,895 | 10,547 |
| Number of independent reflections ($R$int) | 2279 | 2739 |
| Number of parameters | 165 | 205 |
| reflections with $I > 2\sigma(I)$ | 2039 | 2666 |
| Refinement method | Full-matrix least-squares on $F2$ | Full-matrix least-squares on $F2$ |
| Goodness-of-fit (GOF) on $F2$ (S) | 1.06 | 1.05 |
| $R$ [$F2 > 2\sigma$ ($F2$)] | 0.041 | 0. 033 |
| $wR(F2)$ | 0.123 | 0.090 |
| $R_{int}$ | 0.041 | 0.023 |
| Absorption coeff. (mm$^{-1}$) | 0.81 | 0.90 |
| Max/min δ$p$ (e/Å$^3$) | 0.16/-0.18 | 0.12/-0.14 |

(Table 6). The catalytic activity depends strongly on both the structure of the ligand and the action of the anion. Indeed, most ligands have a low absorbance with all the anions except in the case of acetate anion where the values of the absorbance are high (Table 5).

### 3.3.1. 1. Effect of the nature of the anion and the ligand

In the $CH_3COO^-$ case (Fig. 5), **L2**, **L3** and **L4** show high values of absorbance in time. However, from 40 min of reaction, the absorbance starts to decrease for **L2** and **L4** and precipitation of the complex could be the reason for the decrease. In sulfates, nitrates, chlorides and bromides (Figs. 6–9), Cu-**L3** complex seams the best oxidation catalyst with a highest value of rate

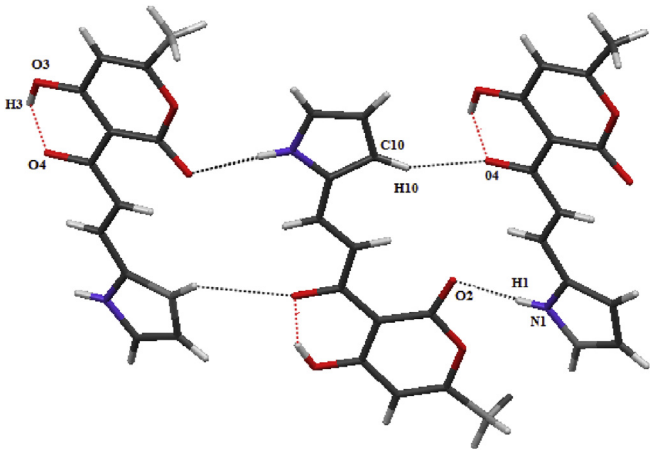


**Fig. 2.** Intermolecular hydrogen bonds in **L3**.

(0.63 μmol L$^{-1}$ min$^{-1}$), whereas, with the other ligands, the rate values calculated are located in the same gap but are still very low within the range of 0.035 μmol L$^{-1}$ min$^{-1}$ (**L1**) to 0.252 μmol L$^{-1}$ min$^{-1}$ (**L4**). Comparison between the catalytic activity of the complexes of copper (II) and the four ligands **L1**, **L2**, **L3** and **L4** (Table 6) showed that Cu-**L1** complexes were observed to be the lowest active, except in the case of $SO_4^{2-}$ anion.

### 3.3.2. Effect of ligand concentration on the catecholase activity

Evolution of catechol oxidation into *o*-quinone is followed by varying the ratio of equivalents ligand **L2**/metallic salt $Cu(CH_3COO)_2$. Three tests were carried out in ratio: 1/1; 2/1 and 1/2.

The results indicate that the test with the ratio **L2**/$Cu(CH_3COO)_2$ = 1 leads to the higher oxidation rate value (31,78 μmol L$^{-1}$ min$^{-1}$). For the ratio 2/1, the maximum value of the rate is 23.91 μmol L$^{-1}$ min$^{-1}$. For the ratio 1/2, the rate value have reached a maximum of 8.93 μmol L$^{-1}$ min$^{-1}$ after 25 mn before decreasing, probably due to complex precipitation in the cell (Fig. 10).

### 3.3.3. Solvent effect

The effect of different solvents (MeOH, DMF and $CH_3CN$) on the oxidation reaction with the ligand **L2** and the $Cu(CH_3COO)_2$ salt was studied under the same thermodynamical conditions. The influence of polar solvents appears clearly through the rate values obtained for the oxidation reaction and the UV–visible records (Table 6; Figs. 11–13). Methanol which is a protic and polar solvent seems to work better than the other two aprotic solvents: acetonitrile and DMF with a maximal value of 31.78 μmol L$^{-1}$ min$^{-1}$ and is in and in agreement with results obtained previously in the literature [36–38] and confirmed that solvatation of copper, by the

**Table 3**
Selected bond lengths (Å) and angles (°) in **L3** and **L4**.

| Bond lengths (Å) | Angles lengths (°) |
|---|---|
| **L3** | |
| N1– $C_9$ 1.374 (16) | C1–$C_6$–$C_7$ 122.78 (11) |
| C6–$C_7$ 1.441 (18) | C6–$C_7$–$C_8$ 122.08 (12) |
| C7–$C_8$ 1.344 (18) | C7–$C_8$–$C_9$ 124.46 (12) |
| C8–$C_9$ 1.426 (18) | C8–$C_9$–$N_1$ 121.53 (11) |
| **L4** | |
| C1–$C_6$ 1.444 (2) | C1–C6–$C_7$ 124.24 (16) |
| C6–$C_7$ 1.440 (2) | C6–$C_7$–$C_8$ 120.39 (17) |
| C7–$C_8$ 1.348 (2) | C7–$C_8$–$C_9$ 128.06 (17) |
| C8–$C_9$ 1.439 (2) | C8–$C_9$–$C_{10}$ 124.18 (15) |

**Table 4**
Bond lengths (Å) of intermolecular hydrogen bonds in L3 and L4.

| Compound | Hydrogen bonds | Distance (Å) | Angles (°) |
|---|---|---|---|
| **L3** | O3–$H_3$ … O4 | 1.683 (2) | 149.57 (2) |
| | N1–$H_1$ … O2 | 1.998 (3) | 175.38 (2) |
| | C10–$H_{10}$ … O4 | 2.706 (3) | 124.41 (3) |
| **L4** | O02–H02 … O01 | 1.661 (2) | 150.03 |
| | C04–H04 … O02 | 2.615 (5) | 152.15 (2) |
| | C015–H015c … O01 | 2.611 (4) | 166.33 (1) |
| | C016–H018a … O03 | 2.639 (12) | 123.86 (2) |
| | C017–H017 … O04 | 2.635 (9) | 163.07 (1) |

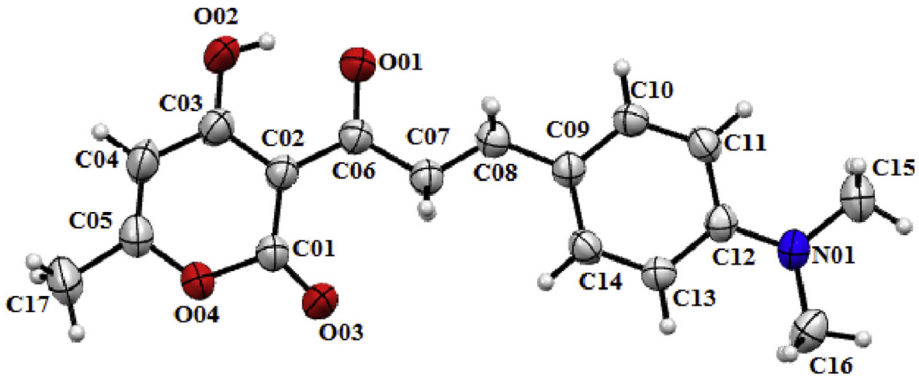


**Fig. 3.** Crystal structure and atoms numbering for **L4**.

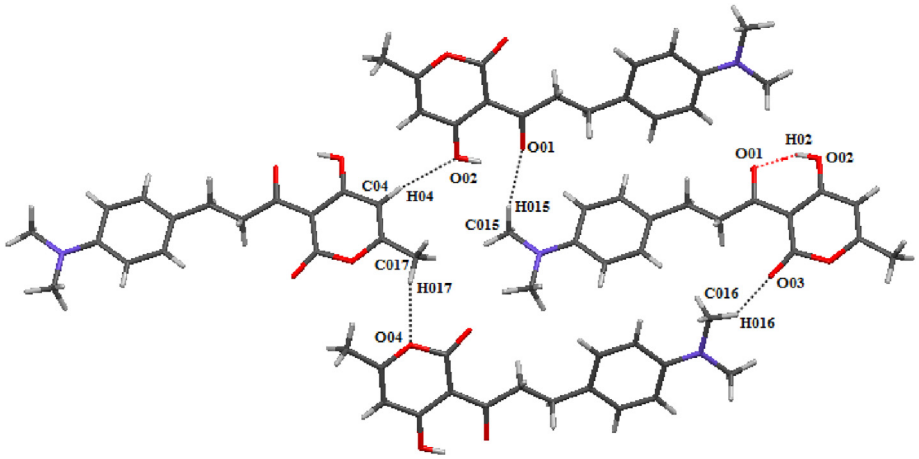


**Fig. 4.** Intermolecular hydrogen bonds in **L4**.

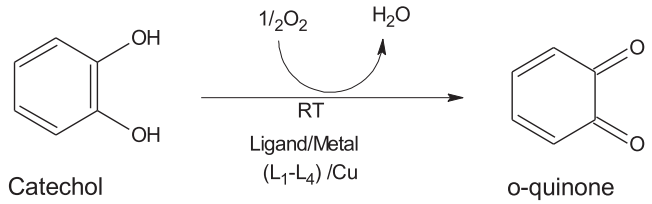


**Scheme 2.**

aprotic and polar solvents (DMF and $CH_3CN$), slows the catalytic activity of the metal cation in the oxidation reaction of catechol to *o*-quinone.

The copper cations are also solvated by the electronegative pole of the solvent but are weaker than the solvation by a hydrogen bond, and became moderately reactive.

## 4. Conclusion

We report here the synthesis of two new chalcone α, β ligands **L1**{ 4-hydroxy-6-methyl-3-[(2E)-3-quinolin-8-ylprop-2-enoyl]-2H-pyran-2-one} and **L2**{ 4-hydroxy-3-[(2E)-3-(1H-indol-3-yl) prop-2-enoyl]-6-methyl-2H-pyran-2-one} with good yields. The X-ray structures of **L3** and **L4** have been investigated for the first time herein. The oxidation reaction of catechol is very efficient to give *o*-quinone by complexes of copper (II), obtained with the four ligands (**L1** − **L4**). Copper (II) complexes were generated in situ and the results obtained show that all the complexes catalyze the aerobic oxidation of catechol to the corresponding *o*-quinone. To understand the parameters influencing the catalytic activity of the studied complexes, the nature and concentration of the ligand and the solvent effects are studied.

**Table 5**
Absorbances of Cu(II) complexes generated in situ after 60 min by mixing metallic salt and ligand L1–L4 (1/1) and catechol.

| Ligand/metallic salt | $Cu(CH_3COO)_2$ | $CuSO_4$ | $Cu(NO_3)_2$ | $CuCl_2$ | $CuBr_2$ |
|---|---|---|---|---|---|
| **L1** | 1,4369 | 0,0058 | 0,0463 | 0,0128 | 0.0229 |
| **L2** | 3,0679 | 0.0076 | 0,0143 | 0.236 | 0.0189 |
| **L3** | 2.6128 | 0.0443 | 0.0618 | 0015 | 0.0115 |
| **L4** | 2.0217 | 0.1287 | 0.1202 | 0.2297 | 0.1972 |

**Table 6**
Oxidation rate of catechol oxidation in methanol (μmol $L^{-1}$ $min^{-1}$).

| Ligand/metallic salt | $Cu(CH_3COO)_2$ | $CuSO_4$ | $Cu(NO_3)_2$ | $CuCl_2$ | $CuBr_2$ |
|---|---|---|---|---|---|
| **L1** | 15.34 | 0.084 | 0.114 | 0.035 | 0.092 |
| **L2** | 31.78 | 0.079 | 0.144 | 0.236 | 0.195 |
| **L3** | 21.05 | 0.456 | 0.630 | 0.252 | 0.560 |
| **L4** | 27.13 | 0.445 | 0.571 | 0.038 | 0.119 |

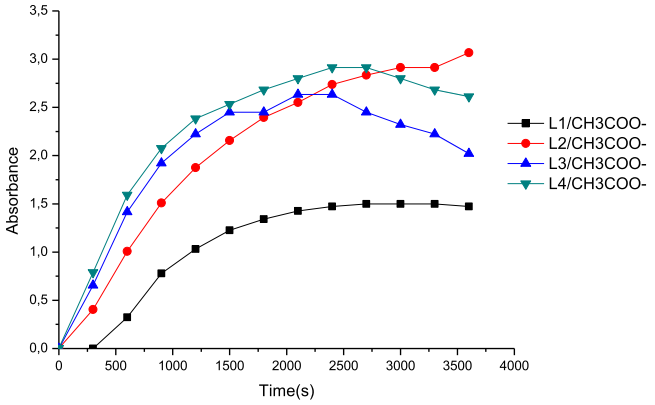


**Fig. 5.** Oxidation of catechol in presence of $Cu(CH_3COO)_2$.

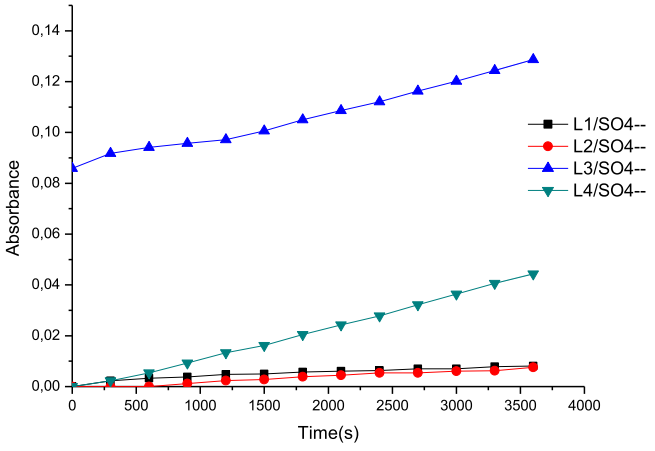


**Fig. 6.** Oxidation of catechol in the presence of sulfate.

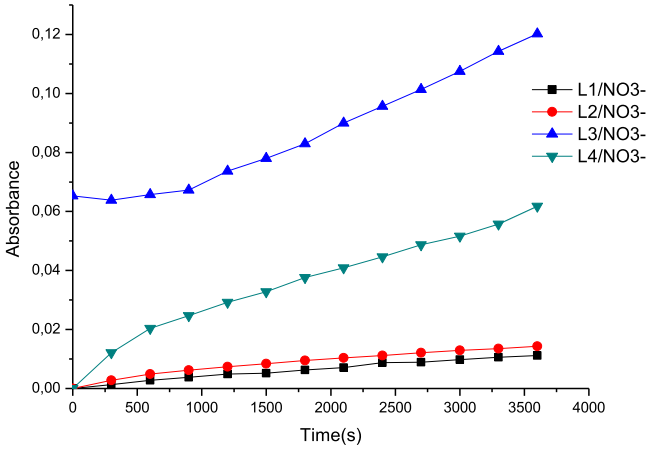


**Fig. 7.** Oxidation of catechol in presence of nitrate.

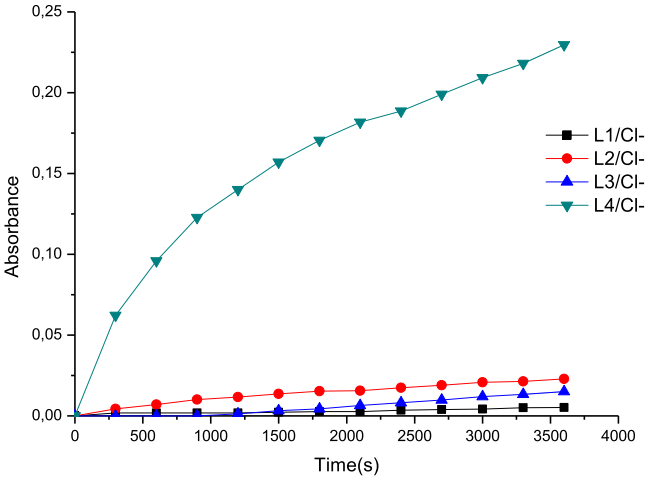


**Fig. 8.** Oxidation of catechol in presence of bromide.

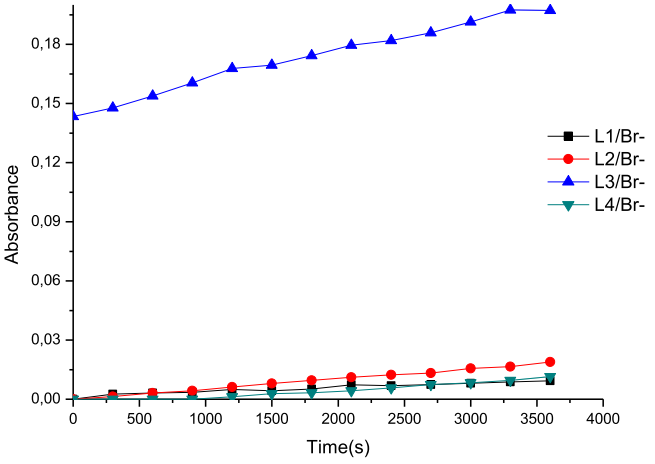


**Fig. 9.** Oxidation of catechol in presence of chloride.

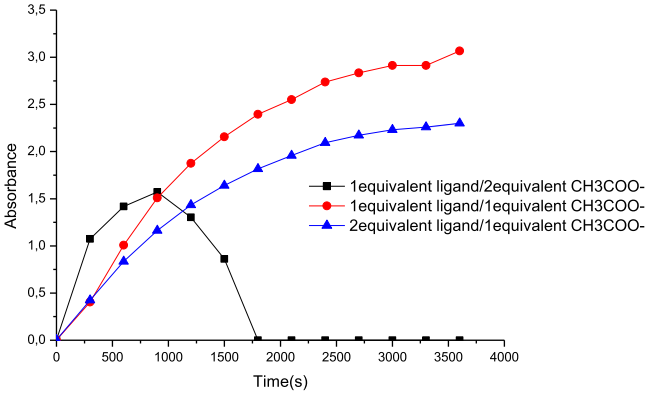


**Fig. 10.** Catechol oxidation in methanol, in presence of formed **L2** copper complexes with different concentrations.

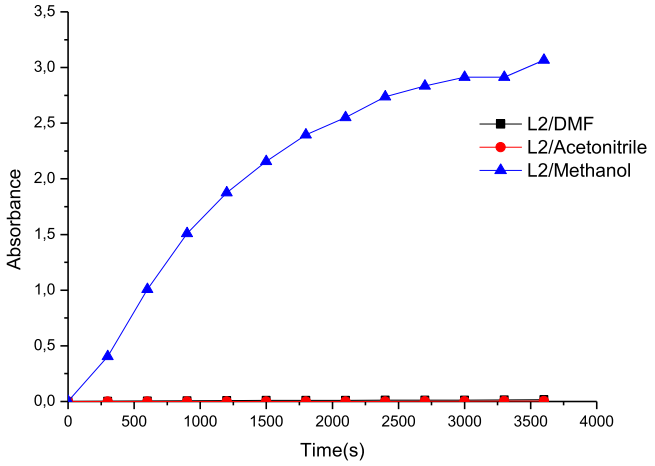


**Fig. 11.** Catechol oxidation in different solvents and in presence of formed **L2** copper Complexes (1 Equivalent of ligand for 1 Equivalent of metallic salt).

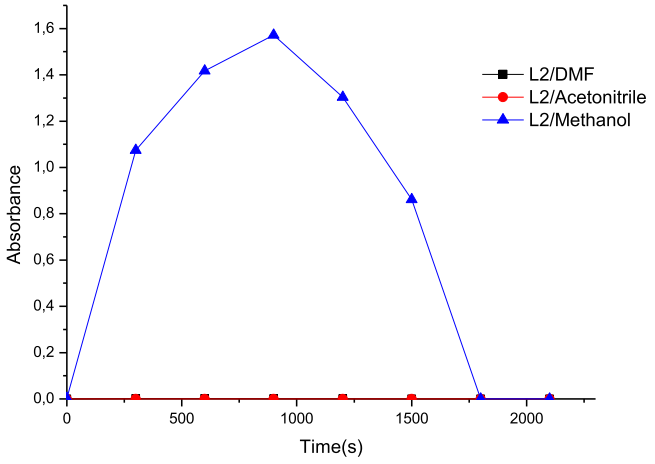


**Fig. 12.** Catechol oxidation in different solvents and in presence of formed **L2** copper complexes (1 Equivalent of ligand for 2 Equivalents of metallic salt).

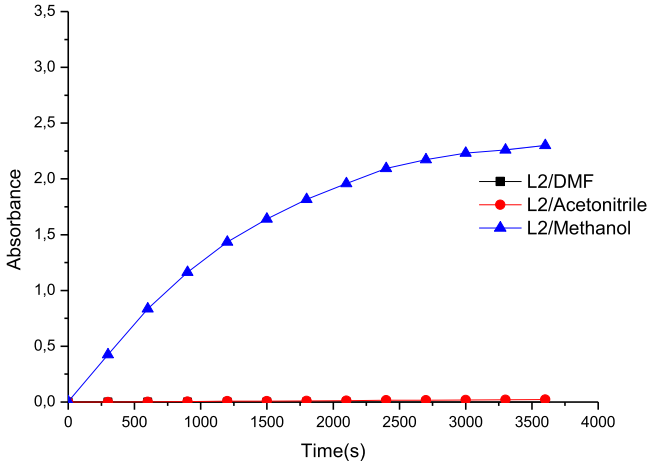


**Fig. 13.** Catechol oxidation in different solvent and in presence of formed **L2** copper Complexes (2 Equivalents of ligand for 1 Equivalent of metallic salt).

## Acknowledgments

We are grateful to the Algerien Ministère de l'Enseignement Supérieur de la Recherche Scientifique (MESRS) and the Algerian Direction Générale de la Recherche Scientifique et du Développement Technologique (DGRSDT) for financial support and to Dr. Jean-Luc Parrain, Dr. Michel Giorgi, Dr Valérie Monnier and Christophe Chendo, from Aix-Marseille Université Campus Saint-Jérôme, France for analyses.

## Electronic supplementary material

CCDC 1000086 and 999631 contain the supplementary crystallographic data for **L3** ($C_{17}H_{17}NO_4$) and **L4** ($C_{13}H_{11}NO_4$), respectively. This data can be obtained free of charge from The Cambridge Crystallographic Data Centre via www.ccdc.cam.ac.uk/data_request/cif.

## References

[1] J. Haggin, Chem. Eng. News 71 (1993) 23.
[2] L.I. Simándi, Catalytic Activation of Dioxygen by Metal Complexes, Kluwer Academic Publishers, Dordrecht, Boston, London, 1992.
[3] A. Biswas, L.K. Das, A. Ghosh, Polyhedron 61 (2013) 253.
[4] M.C. Linder, C.A. Goode, Biochemistry of Copper, Plenum, New York, 1991.
[5] W. Kaim, J. Angew. Chem. Int. Ed. Engl. 35 (1996) 43.
[6] T.N. Sorrel, Tetrahedron 45 (1989) 3.
[7] N. Kitajima, Y. Morooka, J. Chem. Soc. Dalton Trans. 2665 (1993).
[8] N. Kitajima, Y. Morooka, J. Chem. Rev. 94 (1994) 737.
[9] K.D. Karlin, J.D. Hayes, Y. Gultneh, R.W. Cruse, J.W. McKown, J.P. Hutchinson, J. Zubieta, J. Am. Chem. Soc. 106 (1984) 2121.
[10] K.D. Karlin, Y. Gultneh, T. Nicholson, J. Inorg. Chem. 24 (1985) 3727.
[11] R.R. Jacobson, Z. Tyeklar, A. Farooq, K.D. Karlin, S. Liu, J. Zubieta, J. Am. Chem. Soc. 110 (1988) 3690.
[12] Z. Tyeklar, K.D. Karlin, Acc. Chem. Res. 22 (1989) 241.
[13] A. Zerrouki, R. Touzani, S. El Kadiri, Arab. J. Chem. 4 (2010) 459.
[14] C. Gerdemann, C. Eicken, B. Krebs, Acc. Chem. Res. 35 (2002) 7019.
[15] C. Belle, K. Selmeczi, S. Torelli, J.L. Pierre, C. R. Chim. 10 (2007) 271.
[16] A. Rompel, C. Gerdemann, A. Vogel, B. Krebs, Inorganic Chemistry Highlights, 155, Wiley VCH-Verlag, Weinheim, Germany, 2002.
[17] A. Rompel, H. Fischer, K.B. Karenzopoulos, D. Meiwes, F. Zippel, H.F. Nolting, C. Hermes, B. Krebs, H. Witzel, J. Inorg. Biochem. 59 (1995) 715.
[18] B. Krebs, K.B. Karenzopoulos, C. Eicken, A. Rompel, H. Witzel, A. Feldmann, R. Kruth, J. Reim, W. Steinforth, S. Teipel, F. Zippel, S. Schindler, F. Wiesemann, Bioinorganic Chemistry: Transition Metals in Biology and Their Coordination Chemistry, 1997, pp. 616–631.
[19] K. Born, P. Comba, A. Daubinet, A. Fuchs, H. Wadepohl, J. Biol. Inorg. Chem. 12 (2007) 36.
[20] A. Rompel, H. Fischer, D. Meiwes, K.B. Karenzopoulos, R. Dillinger, F. Tuczek, H. Witzel, B. Krebs, J. Biol. Inorg. Chem. 4 (1999) 56.
[21] I.A. Koval, K. Selmeczi, C. Belle, C. Philouze, E. Saint-Aman, I. Gautier-Luneau, A.M. Schuitema, M. Van Vliet, P. Gamez, O. Roubeau, M. Lüken, B. Krebs, M. Lutz, A.L. Spek, J.L. Pierre, J. Reedijk, Chem. A Eur. J. 12 (2006) 6138.
[22] G.M. Sheldrick, SHELXS97 and SHELXL97, Universität Göttingen, Göttingen, Germany, 1997.
[23] G.M. Sheldrick, *SHELX97* – Program for Crystal Structure Analysis (Release 97–2), 1998.
[24] O. Fadel, T. Chelfi, S. Abouricha, Z. Lamzira, N. Benchat, A. Asehraou, Rev. Microbiol. Ind. San. Environ. 4 (2010) 114.
[25] V.N. Patange, B.R. Arbad, Transit. Metal. Chem. 32 (2007) 944.
[26] V.N. Patange, B.R. Arbad, J. Serb. Chem. Soc. 76 (9) (2011) 1237.
[27] A.V. Manaev, K.V. Tambov, V.F. Traven, Russ. J. Org. Chem. 44 (7) (2008) 1054.
[28] V.N. Patange, R.K. Pardeshi, B.R. Arbad, J. Serb. Chem. Soc. 73 (11) (2008) 1073.
[29] H. Allen, O. Kennard, D.G. Watson, L. Brammer, A.G. Orpen, R. Taylor, J. Chem. Soc. Perkin Trans. 2 (1987) S1–S19.
[30] S. Thabti, A. Djedouani, A. Bendaas, S. Boufas, R. Louis, D. Mandon, Acta Cryst. E E69 (2013) 524.
[31] M.N. Tahir, M.N. Ahmed, A.F. Shad, Acta Cryst. E E70 (2014) 1254.
[32] M. El Kodadi, F. Malek, R. Touzani, A. Ramdani, Catal. Commun. 9 (2008) 966.
[33] I. Bouabdallah, R. Touzani, I. Zidane, A. Ramdani, Catal. Commun. 8 (2007) 707.
[34] N. Boussalah, R. Touzani, I. Bouabdallah, S. El Kadiri, S. Ghalem, Int. J. Acta. Res. 2 (2009) 137.
[35] N. Boussalah, R. Touzani, I. Bouabdallah, S. El Kadiri, S. Ghalem, J. Mol. Cat. A Chem. 306 (2009) 113.
[36] A. Mouadili, A. Attayibat, S. El Kadiri, S. Radi, R. Touzani, Appl. Cata. A Gen. 454 (2013) 93.
[37] K.S. Banu, M. Mukherjee, A. Guha, S. Bhattacharya, E. Zangrando, D. Das, Polyhedron 45 (2012) 245.
[38] A. Djedouani, F. Abrigach, M. Khoutoul, A. Mohamadou, A. Bendaas, A. Oussaid, R. Touzani, Orient. J. Chem. 31 (2015) 1.